ACS APPLIED MATERIALS & INTERFACES

Research Article

www.acsami.org

Superhydrophobic Surfaces Fabricated by Femtosecond Laser with Tunable Water Adhesion: From Lotus Leaf to Rose Petal

Jiangyou Long,[†] Peixun Fan,[†] Dingwei Gong,[†] Dafa Jiang,[†] Hongjun Zhang,[†] Lin Li,[‡] and Minlin Zhong*,[†]

[†]Laser Materials Processing Research Centre, School of Materials Science and Engineering, Tsinghua University, Beijing 100084, P.R. China

[‡]Laser Processing Research Centre, School of Mechanical, Aerospace and Civil Engineering, The University of Manchester, Manchester M13 9PL, England

Supporting Information

ABSTRACT: Superhydrophobic surfaces with tunable water adhesion have attracted much interest in fundamental research and practical applications. In this paper, we used a simple method to fabricate superhydrophobic surfaces with tunable water adhesion. Periodic microstructures with different topographies were fabricated on copper surface via femtosecond (fs) laser irradiation. The topography of these microstructures can be controlled by simply changing the scanning speed of the laser beam. After surface chemical modification, these as-prepared surfaces showed superhydrophobicity combined with different adhesion to water. Surfaces with deep microstructures showed self-cleaning properties with extremely low water adhesion, and the water adhesion increased when the surface microstructures became flat. The changes in surface water adhesion are attributed to the transition from Cassie state to Wenzel state. We also demonstrated that these superhydrophobic surfaces with different adhesion can be used for transferring small water droplets without any loss. We demonstrate that our approach provides a novel but simple way to tune the surface adhesion of superhydrophobic metallic surfaces for good potential applications in related areas.

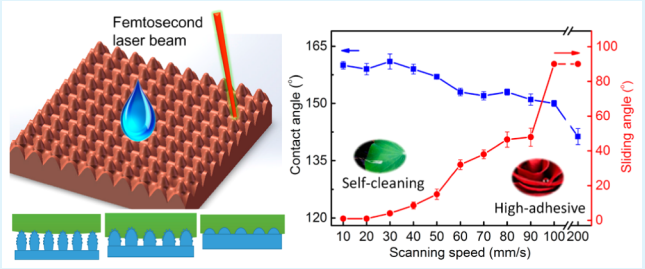

KEYWORDS: *femtosecond laser, superhydrophobic surface, copper, tunable water adhesion, microdroplet manipulation*

INTRODUCTION

Inspired by nature, superhydrophobic surfaces with an apparent contact angle (CA) above 150° have attracted tremendous attention and research efforts in recent years.[1−3] Lotus leaves and rose petals are two typical kinds of superhydrophobic surfaces in nature. Lotus leaves are well-known for the "lotus effect". These surfaces show low adhesion to water. Water droplets cannot remain stable but spontaneously roll off and remove dust particles on the surfaces.[4] On the contrary, rose petals show high adhesion to water, water droplets cannot move at any tilted angles on the surface which is called the "petal effect".[5]

In the past few years, superhydrophobic surfaces have shown great potential applications in many fields, such as self-cleaning surface, oil−water separation, anti-icing surface, and liquid transportation.[6−10] For these applications, controlling the adhesion of the liquid toward the target surface plays a significant role since the adhesive property ultimately determines the dynamic performance of the liquid on the surface. Generally, different adhesions on superhydrophobic surfaces are ascribed to different surface microstructures, which results in different wetting states for water droplets on the surfaces.[11] For example, since the microstructures on rose petals have a larger pitch value than those on the lotus leaf, the liquid is allowed to impregnate between the microstructures but partially penetrates into the nanostructures. This is referred to the Cassie impregnating wetting regime, which leads to the high adhesion of rose petals.[5] Nowadays, many methods, such as self-assembly, the colloidal template technique, electrospinning, and polymer imprinting, have been utilized to fabricate different microstructures to achieve superhydrophobic surfaces with tunable water adhesion.[11−14] Li et al. fabricated five types of CuO microflower/nanorod array structures by a one-step solution-immersion process to achieve superhydrophobic surfaces with different water adhesion.[15] Cheng et al. fabricated ball-like structured $Cu(OH)_2$ with controlled surface microstructures through solution immersion process to tune the surface adhension.[16] Ishii et al. prepared tunable adhesive superhydrophobic surfaces through inducing metal microdomains on superhydrophobic polymer microscopic structured surfaces.[17] Among these proposed methods, however, it is still difficult to modulate the surface topography precisely. Micro-

Received: March 2, 2015
Accepted: April 23, 2015
Published: April 23, 2015

DOI: 10.1021/acsami.5b01870
ACS Appl. Mater. Interfaces 2015, 7, 9858−9865

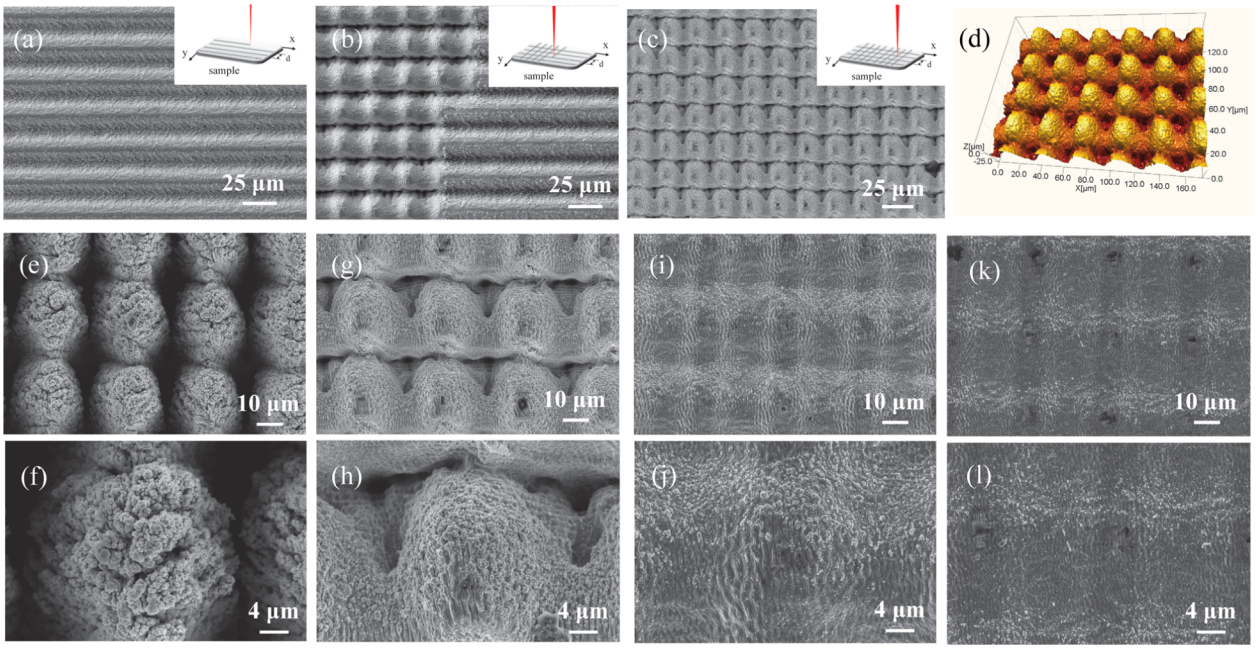

Figure 1. (a–c) Changes in surface morphology during the laser irradiation process. (top right insets) Schematics of the laser scanned paths. (d) Typical 3D images of the laser irradiated surface obtained by a 3D optical profilometer. (e–l) SEM images of the copper surface structured by an fs laser with different scanning speeds: (e, f) 10, (g, h) 50, (i, j) 100, and (k, l) 200 mm s^{-1}.

structure with controlled topographies, which is vital for tuning the surface water adhesion, can only be fabricated by photolithography or other similar mold-based lithographic techniques.[11,18] These techniques suffer from intrinsic shortcomings such as high cost, complexity, and expensive mask fabrication.

Femtosecond (fs) laser micromachining is a one-step direct maskless fabrication technique, which can fabricate versatile hierarchical structures consisting of micro- and nanoscale features on a wide range of materials such as metals,[19−21] glasses,[22] and silicon.[23,24] This technique has been proved to be a promising method to fabricate superhydrophobic surfaces.[25,26] For example, Moradi et al. studied the effect of the process parameters of the femtosecond laser irradiation on the hydrophobicity of the resulting micro/nanopatterned morphologies on stainless steel. They found that most of the laser fabricated surfaces revealed enhanced superhydrophobicity.[20] Yong et al. fabricated a superhydrophobic surface with hierarchical mesh-porous structure by femtosecond irradiation on silicon. The fabricated surfaces showed a superhydrophobic character with water contact angle reaching up to 158° ± 1° and sliding angle to 4° ± 0.5°.[23] However, most of these works only focused on the realization of superhydrophobic surfaces via fs laser irradiation. Little is known about the influence of fs laser fabricated different micro/nanostructures on the surface water adhesion. Even some papers reported the intelligent surfaces with tunable water adhesion fabricated via fs laser irradiation, the main method used was to selectively irradiate the surface by fs lasers.[27−31] The areas irradiated by the fs laser were superhydrophobic due to the laser-induced micro/nanostructures, and the areas without laser irradiation were hydrophobic. The adhesion of the prepared surface was tuned by varying the area ratio of hydrophobic areas to superhydrophobic areas, at the same time, the overall contact angles (CAs) of these surfaces decreased with increased area ratio.

In this paper, we proposed a novel but simple way to fabricate superhydrophobic surfaces with tunable water adhesion via fs laser irradiation. Different from previous works, the tunable water adhesion is achieved by the different surface morphologies induced by fs laser irradiation instead of different area ratios. Hierarchical structures consisting of micro- and nanoscale features with different topographies are obtained by simply changing the scanning speed of an fs laser beam. Different surface morphologies result in different wetting states and then lead to different surface water adhesion. Surfaces with deep microstructures tend to form Cassie state with extremely low water adhesion. When the surface microstructures become flat, the surfaces tend to form Wenzel state with high water adhesion. Our results may further extend the applications of fs laser micromachining for tunable superhydrophobic surfaces.

EXPERIMENTAL SECTION

1. Materials. Copper samples (99.9% purity, 2 mm thick) were mechanically polished to mirror finish and cleaned ultrasonically with ethanol before laser treatment.

2. Laser Irradiation. The as-prepared samples were irradiated with a linearly polarized fs laser (TruMicro series from Trumpf) with wavelength of 1030 nm, repetition rate of 400 kHz, and pulse width about 800 fs. The output laser power was fixed to 4 W. A two mirror galvanometric scanner (hurrySCAN) with an F-Theta objective lens (f = 100 mm) was used to focus and scan the laser beam in the x–y direction. The focused diameter of the Gaussian-profile laser beam at $1/e^2$ of its maximum intensity was approximately 30 μm. The laser processing experiments were performed in atmospheric environment under normal incidence of the laser beam. The laser scanning was performed line-by-line in the horizontal direction (x direction) and then in the vertical direction (y direction). The interval of adjacent laser scanning lines (d as shown in the insets on the top right of Figure 1a–c) was held constant at 30 μm which means there was no overlap between successive lines. In the experiments, we only changed the scanning speed (ν) of the laser beam from 10 to 200 mm s^{-1}; the other laser parameters were kept constant.

DOI: 10.1021/acsami.5b01870
ACS Appl. Mater. Interfaces 2015, 7, 9858−9865

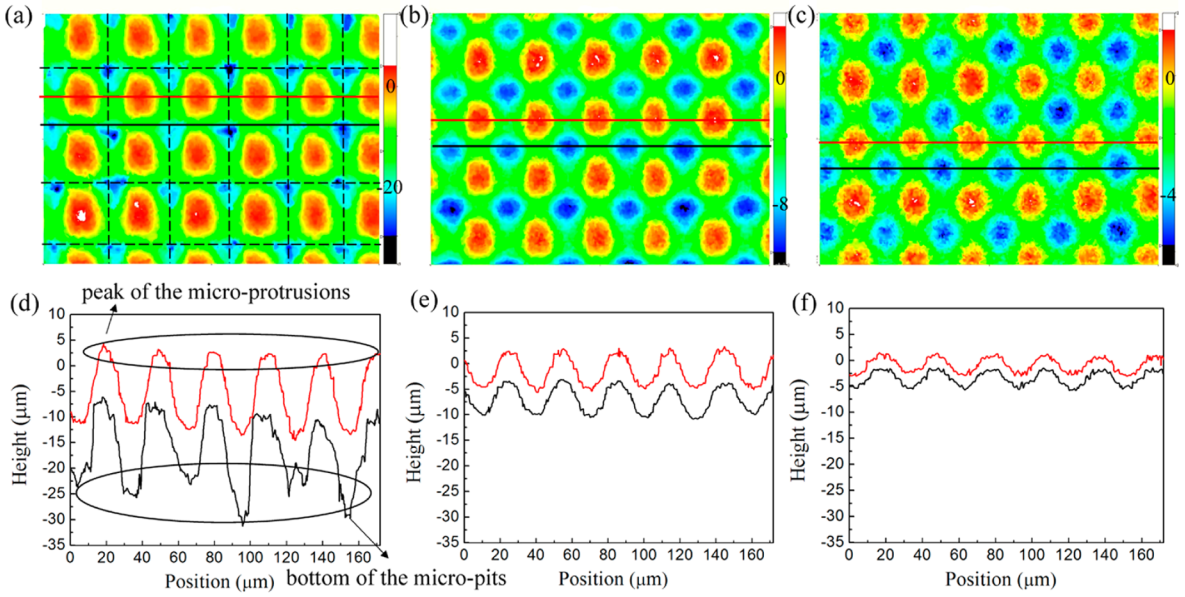

Figure 2. 2D topography map with a scanned area of 172.6 μm × 128.4 μm of the copper surfaces structured by an fs laser with different scanning speeds and the corresponding cross-section profiles: (a, d) 50, (b, e) 100, and (c, f) 200 mm s^{-1}.The black dash lines in part a represent the laser scanned path, and the red and black lines in a–c represent the selected line for profile measurement as shown in d–f.

3. Surface Chemical Modification. After irradiation, the samples were cleaned ultrasonically with ethanol and dried by compressed air. Then the samples were immersed into $CF_3(CF_2)_7CF_2CF_2$–Si-$(OCH_3)_3$ methanol solution with a concentration of 1% for 2 h followed by washing with ethanol and drying in an oven at 80 °C for 30 min.

4. Surface Analysis. The morphologies of the surfaces were analyzed using a LEO-1530 scanning electron microscope (SEM). The topography measurements were performed using a 3D optical profilometer (MicroXAM-3D, ADE technology) with a resolution of 1 nm in the vertical direction.

The wettability of the samples was evaluated by measuring the apparent CAs, advancing CAs, and receding CAs using a video-based optical contact angle-measuring device (OCA 15 Plus from Data Physics Instruments) and the sessile drop technique. The advancing CAs and the receding CAs were acquired through increasing and decreasing the water volume on the surface, respectively. The sliding behavior of the sample was evaluated by measuring the sliding angles (SAs) using the tilting plate method. When the sample was gradually tilted from the horizontal state, the droplet would slide along the inclined surface at a critical slope angle. This angle was define as the sliding angle (SA). The selected water droplet volume for CAs and SAs measurement was 4.5 μL. The adhesive force of the surface was measured through a high-sensitivity microelectromechanical balance (DCAT 11 from Data Physics Instruments). A water droplet (4 μL) was hung on a metal ring fixed to a balance, then the stage with the sample was moved upward at a constant speed of 0.02 mm s^{-1} until the sample lightly touched the droplet, the stage came down again. The maximum force recorded when the droplet was just leaving the surface was defined as the adhesive force.

RESULTS AND DISCUSSION

1. Laser Structured Surfaces. Figure 1 illustrates the changes in surface morphology during laser irradiation and the final microstructures of the laser irradiated copper surfaces with different ν. Since the average laser fluence used is far beyond the ablation threshold, the extra energy enables an overall material removal. The microstructures on the surface are attributed to the fs laser-induced material ablation. The experiments are performed with a Gaussian beam, which has a higher fluence at the center of the circular spot compared to

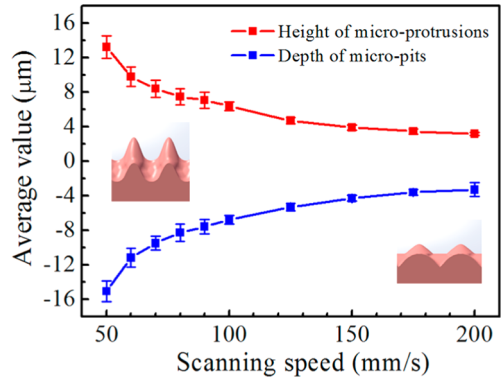

Figure 3. Average height of the microprotrusions and average depth of the micropits as a function of the scanning speed of the fs laser beam, the insets show the schematics of the microstructures on the surfaces.

the edges. Hence, more material is ablated in the center of the laser beam scanned path, which results in the formation of sunken areas and raised areas at the edge of the laser beam scanned path. In our experiments, the laser scanning is performed line-by-line in the horizontal direction at first and then in the vertical direction. As shown in Figure 1a, microgrooves form at the laser scanned paths after the horizontal scanning. As further laser scanning are performed in vertical direction, cone-shaped microprotrusions form at the edge of the laser beam scanned path and micropits form at the intersection of two laser scanned paths because these areas experience more laser shots (Figure 1b). As a result, the laser irradiated surface is characterized with periodic arrays of cone-shaped microprotrusions and micropits (Figure 1c and d, part d is a result by a 3D optical profilometer). Moreover, some particles or folds in nanometer scale also exist on these micrometer scale structures.

As shown in Figure 1e–l, the topography of the copper surfaces changes greatly with different ν. When ν is high, the micrometer scale structures are flat and shallow (Figure 1i–l), their surfaces are mainly composed of some nanofolds and

DOI: 10.1021/acsami.5b01870
ACS Appl. Mater. Interfaces 2015, 7, 9858–9865

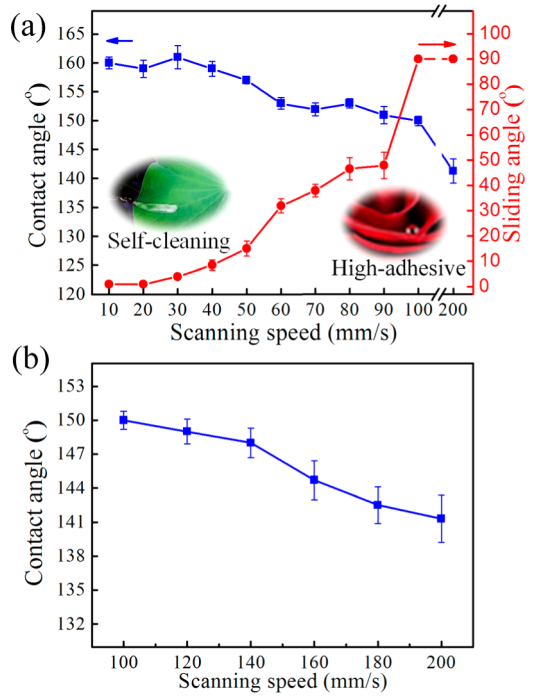

Figure 4. (a) Contact angles and sliding angles of a water droplet on the laser irradiated surfaces with different scanning speeds. (b) Contact angles of a water droplet on the laser irradiated surfaces with high scanning speed (100−200 mm s^1).

redeposited nanoparticles. With decreasing of ν, the height of the microprotrusions and the depth of the micropits increase, and plenty of laser-induced sophisticated nanostructures appear on the surfaces (Figure 1g and h). We further used a 3D optical profilometer to analyze the surface topography. When ν is below 50 mm s^{-1}, the micropits on the surface is so deep that the sample surfaces show a strong light absorption,[32] the surface topography is difficult to measure precisely by the optical profilometer. So we only analyzed the sample surfaces structured with ν higher than 50 mm s^{-1} in our experiments.

As shown in Figure 2, periodic micropits (blue areas in Figure 2a−c) are formed in the center of the laser scanned paths (the dash line in Figure 2a), and periodic microprotrusions (red areas in Figure 2a−c) are formed between two adjacent laser scanned paths. Moreover, the bottom of the micropits locate at the intersection of two laser scanned paths as shown in Figure 2a. Figure 2d−f show the cross-section profiles corresponding to the selected lines in Figure 2a−c, the red lines and black lines represent the cross-section profiles of the periodic microprotrusions and micropits, respectively. It is evident that the period of the periodic microstructures is about 30 μm which is similar to the interval of the adjacent laser scanning lines. Detailed height and depth information is summarized in Figure 3. When ν is 50 mm s^{-1}, the average

Table 1. Advancing Contact Angles (θ_a), Receding Contact Angles (θ_r), and the CAH ($\Delta\theta = \theta_a - \theta_r$) for the Laser Irradiated Surfaces with Different Scanning Speed

	scanning speed (mm/s)				
	10	50	100	150	200
θ_a (deg)	159 ± 1	156 ± 1	150 ± 2	149 ± 3	133 ± 3
θ_r (deg)	157 ± 1	143 ± 1	122 ± 3	119 ± 3	101 ± 4
$\Delta\theta$ (deg)	2	13	28	30	32

height and depth of the microprotrusions and micropits are about 13.3 ± 1.3 and 15.1 ± 1.3 μm, respectively. However, as ν increases to 100 and 200 mm s^{-1}, the average height of the microprotrusions decreases to 6.4 ± 0.5 and 3.2 ± 0.2 μm, and the average depth of the micropits decreases to 6.8 ± 0.5 and 3.3 ± 0.8 μm, respectively. It can be seen that, by simply changing the scanning speed of the laser beam, the topography of the surface is tuned precisely.

2. Superhydrophobicity. To show how the wetting property is affected by the surface topography, after surface chemical modification, the CAs and SAs of the laser irradiated surfaces are illustrated in Figure 4. When ν is lower than 100 mm s^{-1}, the laser irradiated surfaces all show superhydrophobicity with an apparent CA above 150°. Further increasing of ν decreases the CAs. In contrast, the SAs increase dramatically with increasing of ν. When the ν is lower than 30 mm s^{-1}, the SAs are less than 10°, which indicates a superhydrophobic surface with self-cleaning property. These surfaces show an excellent superhydrophobic property and very weak adhesion between the sample and water droplet. As shown in Figure 5a, we gradually upward moved a laser irradiated surface (scanned with a ν of 10 mm s^{-1}) to contact a 4 μL water droplet suspended on an ultrafine microsyringe (the external diameter is only 0.23 mm). However, the sample could be easily moved away from the water droplet with very little pulling-down force, indicating that the adhesion between the sample and the droplet is very weak. With the ν increases to 60, 80, and 100 mm s^{-1}, the SAs increase to 31 ± 3°, 47 ± 4°, and 90°, respectively. In the case that the SA equals to 90°, the water droplets are firmly pinned on the superhydrophobic surface without any movement at any tilted angles as shown in Figure 5b. The results in video S1 (see the Supporting Information) show more clearly the different SAs of different samples. Five areas on the copper surfaces were irradiated by the fs laser with different ν, and two water droplets with a volume of 4.5 μL were placed on each area. The copper plate was tilted gradually from a horizontal position to a nearly vertical position. As a result, the water droplets on different areas rolled down from the plate sequentially.

In this work, the contact angle hysteresis (CAH) for the water droplets on these surfaces are also investigated. As shown in Table 1, with an increase in the ν of the fs laser, the CAH increases dramatically.

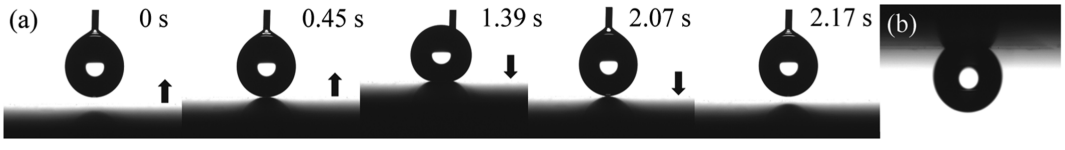

Figure 5. (a) Sequential photographs of the laser irradiated surface (with a scanning speed of 10 mm s^{-1}) contacts and then departs from a water droplet of 4 μL suspended on a syringe. The black arrows correspond to the substrate's moving direction. (b) Shape of a water droplet on the laser irradiated surface (with a scanning speed of 100 mm s^{-1}) when it is turned upside down.

DOI: 10.1021/acsami.5b01870
ACS Appl. Mater. Interfaces 2015, 7, 9858−9865

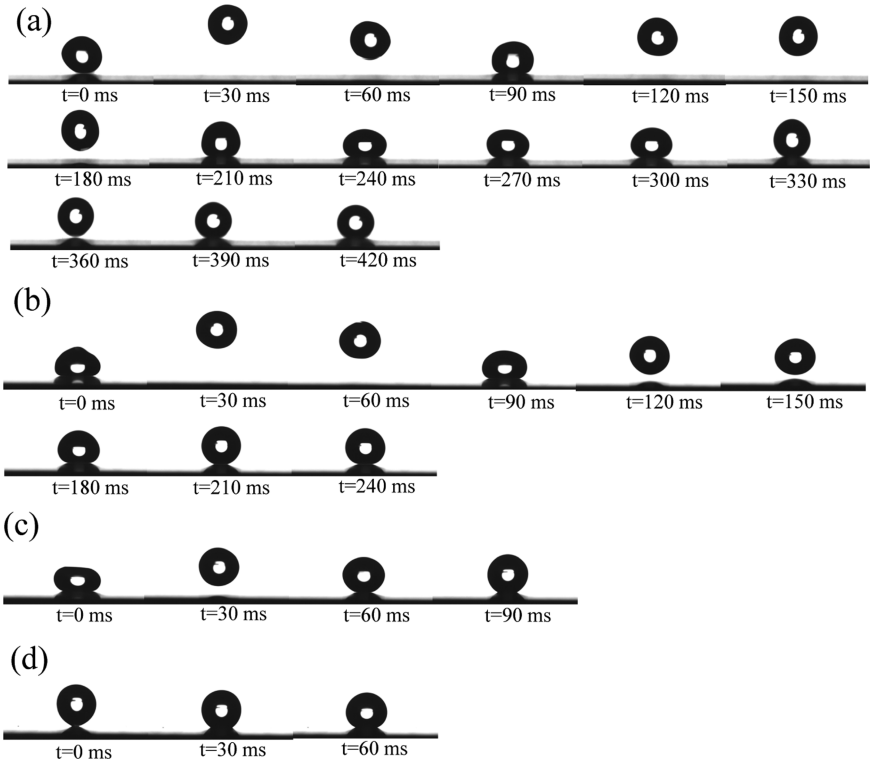

Figure 6. Snapshots of a water droplet impacting the laser irradiated surfaces with different scanning speeds: (a) 10, (b) 50, (c) 70, (d) 100 mm s^{-1}.

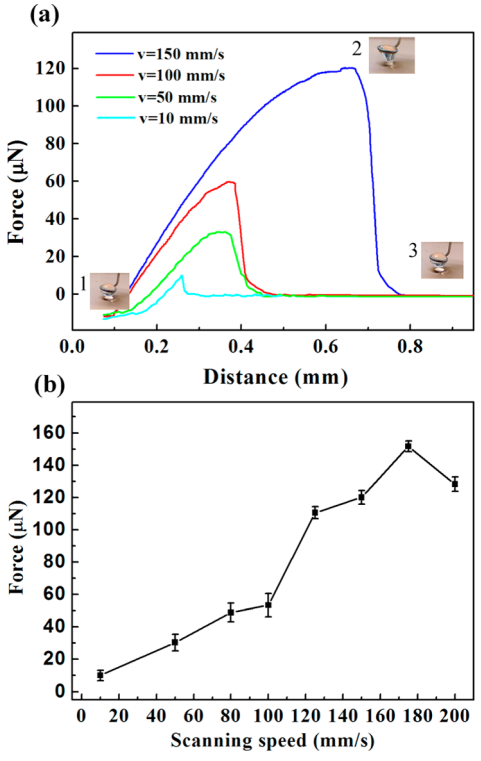

Figure 7. (a) Typical force–distance curves on the as-prepared surface. (inset) Photographs for typical measurement processes: (1) a water droplet was in slight contact with the sample surface, (2) the sample was slowly moved down, (3) the water droplet left the sample surface. (b) Dependence of the adhesive force on the laser scanning speed.

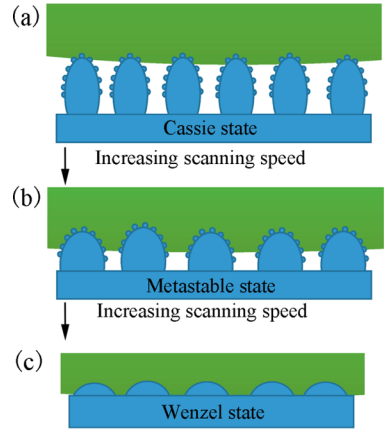

Figure 8. Schematic illustration of a water droplet in contact with the as-prepared samples in (a) the Cassie state, (b) the metastable state, and (c) the Wenzel state.

In addition to the measurements on CAs, SAs, and CAH, a bouncing experiment by a water droplet free falling from a certain height onto the object surface was conducted in this study to further characterize different superhydrophobic surfaces.[33,34] A 5 μL water droplet was released from a height of 30 mm above the surface, then the rebound time which represents the different adhesion property of different samples was recorded. As shown in Figure 6, when ν is 10 mm s^{-1}, the water droplet rebounds 3 times from the surface due to its extremely low adhesion to water. As ν increases to 50 and 70 mm s^{-1}, the water droplet only rebounds for 2 and 1 times, respectively. Further increasing the ν to 100 mm^{-1}, the droplet sticks to the surface without any rebound (Figure 6d), which indicates a high adhesion to water. These results further prove the different adhesion to water of these laser irradiated surfaces.

DOI: 10.1021/acsami.5b01870
ACS Appl. Mater. Interfaces 2015, 7, 9858–9865

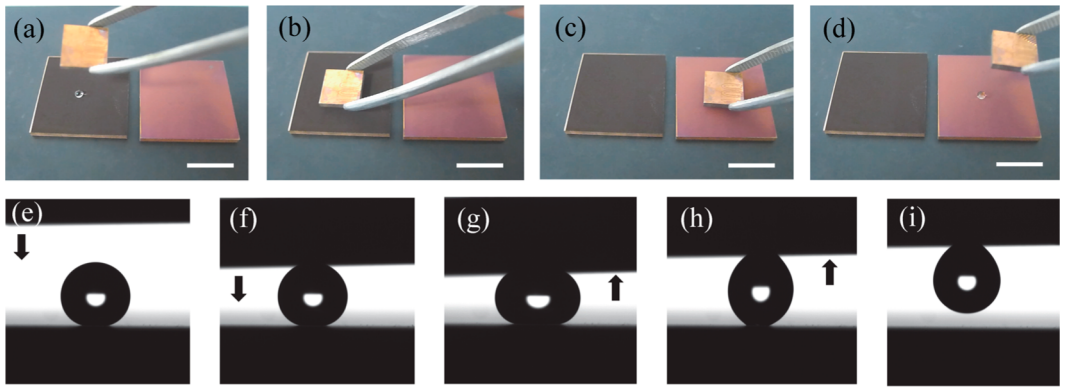

Figure 9. (a–d) Screenshot of transferring a 5 μL water droplet from the low adhesive superhydrophobic surface (ν = 10 mm s^{-1}, the left sample in the picture) to the high adhesive superhydrophobic surface (ν = 150 mm s^{-1}, the right sample in the picture) by another superhydrophobic surface with middle adhesive force to water (ν = 100 mm s^{-1}, the small sample in the picture). The scale bars are 1 cm. (e–i) Photographs for a water droplet (5 μL) during no lost transport from the low adhesive superhydrophobic surface (ν = 10 mm s^{-1}) to the high adhesive superhydrophobic surface (ν = 100 mm s^{-1}). The black arrows correspond to the moving direction of the above sample.

A high-sensitivity microelectromechanical balance system was used to investigate accurately the surface adhesion of the laser irradiated surfaces. Figure 7a shows the typical force–distance curves for the as-prepared surfaces. When the sample surface contacted the water droplet on the metal ring, the distance was recorded as 0. Then the sample was slowly moved down, the distance and force between the sample surface and the water droplet began to increase. A maximum force recorded when the droplet was just leaving the surface, defined as the adhesive force. It is shown that when ν decreases, the adhesive force decreases dramatically. For the as-prepared sample with a ν of 125 mm s^{-1}, the adhesive force is 110 μN which is much larger than that of the natural peanut leaf with an adhesive force of only 70 μN.[35] However, as the ν decreases to 100, 80, and 50 mm s^{-1}, the adhesive force decreases in corresponding to 53, 49, and 30 μN, respectively. Further decreasing the ν to 10 mm s^{-1}, the adhesive force between the microdroplet and the sample surface is only 10 μN.

3. Discussion about the Mechanism. In general, two models are used to describe the solid–liquid interaction: (1) the liquid completely fills the valleys of a rough solid surface (Wenzel state), and (2) it leaves air inside the valleys of the rough solid surface (Cassie state).[3] In our experiments, when ν is low (below 30 mm s^{-1}), the surface shows superhydrophobicity with large CA, low CAH, and low SA, which is similar to lotus leaf. This excellent superhydrophobicity can be explained by Cassis model as shown in Figure 8a. Because the surface have a large roughness consisting of deep microstructures combined with rich nanostructures, a layer of air is trapped between the surface and the droplet. It is a nonhomogeneous or composite regime with a three-phase solid–water–air interface. In this state, the "air" parts of the surface can be considered perfectly nonwetting.[16] Thus, it leads eventually to an extremely low water adhesion. As ν increases, the surface microstructures become shallow, the water can partly get into the grooves of the rough solid surface which is attributed to the capillary effect of the cone-shaped microstructures,[36] and the liquid–solid contact area appears as shown in Figure 8b. This state between Cassie and Wenzel states is named the metastable or combined state in some papers.[3,37] The increased liquid–solid contact area results in an enlarged adhesion to water.[38−40] When the ν increases to 100 mm s^{-1}, the laser irradiated surface is similar to the surface of rose petals. As reported by Feng et al., the surface of a red rose petal consists a periodic array of micropapillae with an average diameter of 16 μm and height of 7 μm.[5] These micropapillae exhibit cuticular folds with a width of 730 nm on each top. As shown in Figure 1i and j, periodic microprotrusions and micropits are observed on the laser irradiated surfaces when the ν is 100 mm s^{-1}. The period of these microstructures is 30 μm and the height of the microprotrusions is 6.8 μm. There are also some nanofolds on these microprotrusions. Moreover, the adhesive force of the rose petal is 63.8 μN, which is very similar to the laser irradiated surface with a ν of 100 mm s^{-1} whose adhesive force is 53 μN.[41] On this surface, water could impregnate between microstructures, but it still does not completely wet into the nanostructures, resulting in high adhesion while maintaining high apparent CA.[42,43] Further increasing the ν to above 120 mm s^{-1}, the surface microstructures become very flat and there are not many nanoscale structures on it. The decreased CAs and high adhesive force of these surfaces can be explained according to the Wenzel model. As illustrated in Figure 8c, the water can get into the grooves of the rough solid surface completely. In the Wenzel model, the CA is related to surface roughness. Increasing the ν results in the decreased surface roughness. Thus, the CA decreases rapidly as shown in Figure 4b.

4. Application. These superhydrophobic surfaces with tunable water adhesion can be used in many fields, such as a "mechanical hand" for the transfer of small water droplets without any loss or contamination for microsample analysis. As shown in Figure 9a, a 5 μL water droplet is first placed on the as-prepared low adhesive superhydrophobic surface with a CA of 160° and a SA of 1°. Then, we use the as-prepared high adhesive superhydrophobic surface to touch the droplet. The water droplet is adhered to the surface and thereby successfully transferred from the low adhesive superhydrophobic surface to the high adhesive superhydrophobic surface (Figure 9b). Subsequently, the high adhesive superhydrophobic surface carries the water droplet to contact with another high adhesive surface (Figure 9c), and this water droplet is released on it (Figure 9d). Furthermore, it is also shown in Figure 9e–i how a 5 μL water droplet can be transferred from a low adhesive surface to a high adhesive surface without any loss.

DOI: 10.1021/acsami.5b01870
ACS Appl. Mater. Interfaces 2015, 7, 9858–9865

CONCLUSIONS

In conclusion, we demonstrated a simple method to realize superhydrophobic surfaces with various adhesion properties to water by tuning the topography of the surface microstructures. Using an fs laser, periodic microstructures with different heights and depths were obtained by simply changing the scanning speed of the laser beam. After surface modification, these surfaces showed superhydrophobicity combined with different adhesion to water. Their SAs can be controlled from 1° to above 90°, and the adhesive force between the surface and the water droplet can be adjusted from low to very high. The tunable water adhesion can be ascribed to the transition from Cassie model to Wenzel model which results from different microstructures on the surfaces. We demonstrated that our results can be helpful for a better comprehension on how the microstructures affect the surface adhesion to water and provided a novel but simple way to tune the surface adhesion of metal surfaces.

ASSOCIATED CONTENT

Supporting Information

Movie S1 showing droplet movement on different surfaces. The Supporting Information is available free of charge on the ACS Publications website at DOI: 10.1021/acsami.5b01870.

AUTHOR INFORMATION

Corresponding Author

*E-mail address: zhml@tsinghua.edu.cn. Tel: +86-10-62789525. Fax: +86-10-6277-3862.

Notes

The authors declare no competing financial interest.

ACKNOWLEDGMENTS

The authors greatly thank the funding support by National Natural Science Foundation of China (51210009), the National Key Basic Research and Development Program of China (2011CB013000).

REFERENCES

(1) Liu, K. S.; Yao, X.; Jiang, L. Recent Developments in Bio-Inspired Special Wettability. *Chem. Soc. Rev.* **2010**, *39*, 3240−3255.
(2) Feng, L.; Li, S. H.; Li, Y. S.; Li, H. J.; Zhang, L. J.; Zhai, J.; Song, Y. L.; Liu, B. Q.; Jiang, L.; Zhu, D. B. Super-Hydrophobic Surfaces: From Natural to Artificial. *Adv. Mater.* **2002**, *14*, 1857−1860.
(3) Roach, P.; Shirtcliffe, N. J.; Newton, M. I. Progress in Superhydrophobic Surface Development. *Soft Matter* **2008**, *4*, 224−240.
(4) Liu, K. S.; Jiang, L. Bio-Inspired Self-Cleaning Surfaces. *Annu. Rev. Mater. Res.* **2012**, *42*, 231−263.
(5) Feng, L.; Zhang, Y. A.; Xi, J. M.; Zhu, Y.; Wang, N.; Xia, F.; Jiang, L. Petal Effect: A Superhydrophobic State with High Adhesive Force. *Langmuir* **2008**, *24*, 4114−4119.
(6) Liu, K. S.; Jiang, L. Metallic Surfaces with Special Wettability. *Nanoscale* **2011**, *3*, 825−838.
(7) Yao, X.; Song, Y.; Jiang, L. Applications of Bio-Inspired Special Wettable Surfaces. *Adv. Mater.* **2011**, *23*, 719−734.
(8) Miljkovic, N.; Wang, E. N. Condensation Heat Transfer on Superhydrophobic Surfaces. *MRS Bull.* **2013**, *38*, 397−406.
(9) Pan, Q.; Wang, M. Miniature Boats with Striking Loading Capacity Fabricated from Superhydrophobic Copper Meshes. *ACS Appl. Mater. Interfaces* **2009**, *1*, 420−423.
(10) Cao, L.; Jones, A. K.; Sikka, V. K.; Wu, J.; Gao, D. Anti-Icing Superhydrophobic Coatings. *Langmuir* **2009**, *25*, 12444−12448.
(11) Bhushan, B.; Her, E. K. Fabrication of Superhydrophobic Surfaces with High and Low Adhesion Inspired from Rose Petal. *Langmuir* **2010**, *26*, 8207−8217.
(12) Cheng, Z. J.; Hou, R.; Du, Y.; Lai, H.; Fu, K. W.; Zhang, N. Q.; Sun, K. N. Designing Heterogeneous Chemical Composition on Hierarchical Structured Copper Substrates for the Fabrication of Superhydrophobic Surfaces with Controlled Adhesion. *ACS Appl. Mater. Interfaces* **2013**, *5*, 8753−8760.
(13) Li, J.; Jing, Z. J.; Yang, Y. X.; Zha, F.; Yan, L.; Lei, Z. Q. Reversible Low Adhesive to High Adhesive Superhydrophobicity Transition On ZnO Nanoparticle Surfaces. *Appl. Surf. Sci.* **2014**, *289*, 1−5.
(14) Jin, M. H.; Feng, X. J.; Feng, L.; Sun, T. L.; Zhai, J.; Li, T. J.; Jiang, L. Superhydrophobic Aligned Polystyrene Nanotube Films with High Adhesive Force. *Adv. Mater.* **2005**, *17*, 1977−1981.
(15) Li, J. A.; Liu, X. H.; Ye, Y. P.; Zhou, H. D.; Chen, J. M. Fabrication of Superhydrophobic CuO Surfaces with Tunable Water Adhesion. *J. Phys. Chem. C* **2011**, *115*, 4726−4729.
(16) Cheng, Z. J.; Du, M.; Lai, H.; Zhang, N. Q.; Sun, K. N. From Petal Effect to Lotus Effect: A Facile Solution Immersion Process for the Fabrication of Super-Hydrophobic Surfaces with Controlled Adhesion. *Nanoscale* **2013**, *5*, 2776−2783.
(17) Ishii, D.; Yabu, H.; Shimomura, M. Novel Biomimetic Surface Based on a Self-Organized Metal-Polymer Hybrid Structure. *Chem. Mater.* **2009**, *21*, 1799−1801.
(18) Wu, D.; Wang, J.; Wu, S.; Chen, Q.; Zhao, S.; Zhang, H.; Sun, H.; Jiang, L. Three-Level Biomimetic Rice-Leaf Surfaces with Controllable Anisotropic Sliding. *Adv. Funct. Mater.* **2011**, *21*, 2927−2932.
(19) Kietzig, A. M.; Hatzikiriakos, S. G.; Englezos, P. Patterned Superhydrophobic Metallic Surfaces. *Langmuir* **2009**, *25*, 4821−4827.
(20) Moradi, S.; Kamal, S.; Englezos, P.; Hatzikiriakos, S. G. Femtosecond Laser Irradiation of Metallic Surfaces: Effects of Laser Parameters on Superhydrophobicity. *Nanotechnology* **2013**, *24*, 415302.
(21) Wu, B.; Zhou, M.; Li, J.; Ye, X.; Li, G.; Cai, L. Superhydrophobic Surfaces Fabricated by Microstructuring of Stainless Steel Using a Femtosecond Laser. *Appl. Surf. Sci.* **2009**, *256*, 61−66.
(22) Ahsan, M. S.; Dewanda, F.; Lee, M. S.; Sekita, H.; Sumiyoshi, T. Formation of Superhydrophobic Soda-Lime Glass Surface Using Femtosecond Laser Pulses. *Appl. Surf. Sci.* **2013**, *265*, 784−789.
(23) Yong, J.; Yang, Q.; Chen, F.; Zhang, D.; Bian, H.; Ou, Y.; Si, J.; Du, G.; Hou, X. Stable Superhydrophobic Surface with Hierarchical Mesh-Porous Structure Fabricated by a Femtosecond Laser. *Appl. Phys. A: Mater. Sci. Process.* **2013**, *111*, 243−249.
(24) Her, T. H.; Finlay, R. J.; Wu, C.; Deliwala, S.; Mazur, E. Microstructuring of Silicon with Femtosecond Laser Pulses. *Appl. Phys. Lett.* **1998**, *73*, 1673−1675.
(25) Chen, F.; Zhang, D.; Yang, Q.; Yong, J.; Du, G.; Si, J.; Yun, F.; Hou, X. Bioinspired Wetting Surface Via Laser Microfabrication. *ACS Appl. Mater. Interfaces* **2013**, *5*, 6777−6792.
(26) Jagdheesh, R.; Pathiraj, B.; Karatay, E.; Romer, G. In'T Veldt, A. Laser-Induced Nanoscale Superhydrophobic Structures On Metal Surfaces. *Langmuir* **2011**, *27*, 8464−8469.
(27) Zhang, D. S.; Chen, F.; Yang, Q.; Yong, J. L.; Bian, H.; Ou, Y.; Si, J. H.; Meng, X. W.; Hou, X. A Simple Way to Achieve Pattern-Dependent Tunable Adhesion in Superhydrophobic Surfaces by a Femtosecond Laser. *ACS Appl. Mater. Interfaces* **2012**, *4*, 4905−4912.
(28) Yong, J. L.; Yang, Q.; Chen, F.; Zhang, D. S.; Du, G. Q.; Bian, H.; Si, J. H.; Yun, F.; Hou, X. Superhydrophobic PDMS Surfaces with Three-Dimensional (3D) Pattern-Dependent Controllable Adhesion. *Appl. Surf. Sci.* **2014**, *288*, 579−583.
(29) Yong, J.; Yang, Q.; Chen, F.; Zhang, D.; Farooq, U.; Du, G.; Hou, X. A Simple Way to Achieve Superhydrophobicity, Controllable Water Adhesion, Anisotropic Sliding, and Anisotropic Wetting Based On Femtosecond-Laser-Induced Line-Patterned Surfaces. *J. Mater. Chem. A* **2014**, *2*, 5499−5507.

DOI: 10.1021/acsami.5b01870
ACS Appl. Mater. Interfaces 2015, 7, 9858−9865

(30) Yong, J.; Chen, F.; Yang, Q.; Zhang, D.; Bian, H.; Du, G.; Si, J.; Meng, X.; Hou, X. Controllable Adhesive Superhydrophobic Surfaces Based on PDMS Microwell Arrays. *Langmuir* **2013**, *29*, 3274−3279.
(31) Yong, J.; Chen, F.; Yang, Q.; Zhang, D.; Du, G.; Si, J.; Yun, F.; Hou, X. Femtosecond Laser Weaving Superhydrophobic Patterned PDMS Surfaces with Tunable Adhesion. *J. Phys. Chem. C* **2013**, *117*, 24907−24912.
(32) Fan, P.; Zhong, M.; Li, L.; Huang, T.; Zhang, H. Rapid Fabrication of Surface Micro/Nano Structures with Enhanced Broadband Absorption on Cu by Picosecond Laser. *Opt. Express* **2013**, *21*, 11628−11637.
(33) Zhang, Q. B.; Xu, D.; Hung, T. F.; Zhang, K. Facile Synthesis, Growth Mechanism and Reversible Superhydrophobic and Superhydrophilic Properties of Non-Flaking CuO Nanowires Grown From Porous Copper Substrates. *Nanotechnology* **2013**, *24*, 065602.
(34) Jung, Y. C.; Bhushan, B. Dynamic Effects of Bouncing Water Droplets on Superhydrophobic Surfaces. *Langmuir* **2008**, *24*, 6262−6269.
(35) Yang, S.; Ju, J.; Qiu, Y.; He, Y.; Wang, X.; Dou, S.; Liu, K.; Jiang, L. Peanut Leaf Inspired Multifunctional Surfaces. *Small* **2014**, *10*, 294−299.
(36) Bico, J.; Thiele, U.; Quere, D. Wetting of Textured Surfaces. *Colloids Surf., A* **2002**, *206*, 41−46.
(37) Lv, P.; Xue, Y.; Shi, Y.; Lin, H.; Duan, H. Metastable States and Wetting Transition of Submerged Superhydrophobic Structures. *Phys. Rev. Lett.* **2014**, *112*, 196101.
(38) Lafuma, A.; Quere, D. Superhydrophobic States. *Nat. Mater.* **2003**, *2*, 457−460.
(39) Marmur, A. The Lotus Effect: Superhydrophobicity and Metastability. *Langmuir* **2004**, *20*, 3517−3519.
(40) Zheng, Y.; Gao, X.; Jiang, L. Directional Adhesion of Superhydrophobic Butterfly Wings. *Soft Matter* **2007**, *3*, 178−182.
(41) Xi, J.; Jiang, L. Biomimic Superhydrophobic Surface with High Adhesive Forces. *Ind. Eng. Chem. Res.* **2008**, *47*, 6354−6357.
(42) Bormashenko, E.; Starov, V. Impact of Surface Forces On Wetting of Hierarchical Surfaces and Contact Angle Hysteresis. *Colloid Polym. Sci.* **2013**, *291*, 343−346.
(43) Bhushan, B.; Nosonovsky, M. The Rose Petal Effect and the Modes of Superhydrophobicity. *Philos. Trans. R. Soc., A* **2010**, *368*, 4713−4728.

DOI: 10.1021/acsami.5b01870
ACS Appl. Mater. Interfaces 2015, 7, 9858−9865